

Quantification and enhancement of image reconstruction accuracy by frequency encoding of spatial information

Harry L. Graber and R. L. Barbour

Department of Pathology, SUNY Downstate Medical Center, Box 25, 450 Clarkson Avenue, Brooklyn, NY 11203

Telephone: (718) 270-1286. Fax: (718) 270-1305. E-mail: hgraber@downstate.edu

Yaling Pei

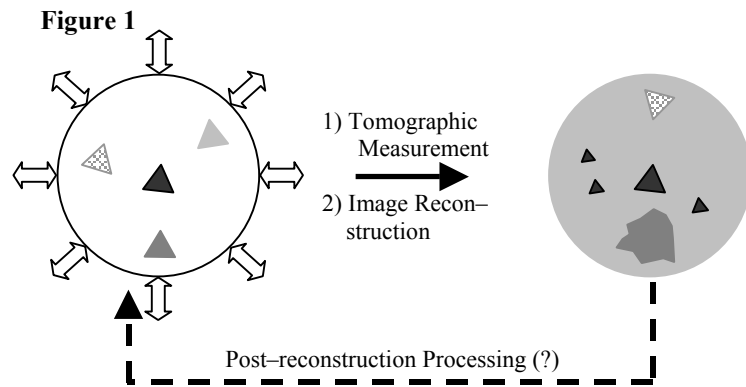
NIRx Medical Technologies Corp., 15 Cherry Lane, Glen Head, NY 11545

Abstract: A method, built around dynamic optical tomography techniques, for quantifying the degree to which image reconstruction algorithms correctly map the spatial locations of a medium's optical coefficients into the image domain, is described.

OCIS codes: (170.3880) Medical and biological imaging; (100.2960) Image analysis; (100.2980) Image enhancement

1. Introduction/Methods

In a set of recent reports, a number of image reconstruction methods [1,2] well suited to the integrated data collection and analysis system [3-5] we are developing for dynamic diffuse optical tomography (DYNOT) [6,7] were presented. These particular algorithms, which are modifications of a standard linear perturbation approach to image recovery, were devised to address several distinct concerns: the requirement for producing a large number of images in a usefully short time, and the practical reality that the systems of equations that arise in diffuse optical tomography (DOT) usually are both underdetermined and highly ill-conditioned. Here we present a recently developed technique for analyzing the action of the reconstruction methods.



inaccurately represented in the image domain.

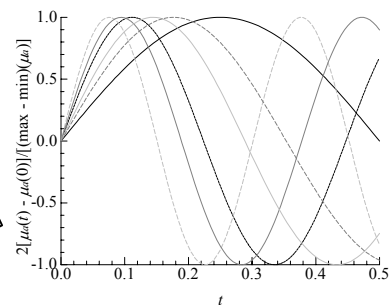
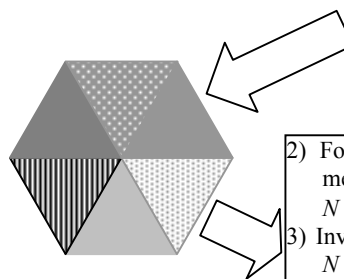
In the absence of information regarding the ISF, there is no apparent way of systematizing the process of modifying a reconstruction algorithm in response to the observed quality of its performance. The approach we have adopted for characterizing the ISF for a given combination of reconstruction algorithm and reference medium is called frequency encoding of spatial information (FESI). It is similar in concept to the phase encoding of spatial information commonly used in magnetic resonance imaging. The steps involved in a FESI calculation are outlined in Figure 2.

The present report is a preliminary demonstration of the utility of the FESI technique. The method has been applied to two different image time series, both

One of the factors that has made algorithm development difficult in the past has been the absence of a way to quantitatively characterize the "information spread function" (ISF) associated with a given image reconstruction method. The term ISF here refers to the precise manner in which the optical coefficients that actually are present in a given location of a target medium are mapped into the spatial domain of the image. Shown in Figure 1 is a cartoon illustrating several ways in which the spatial dependence of a medium's properties can be

Figure 2

1) Assign a modulation frequency to each element's μ_a



- 2) Forward problem: compute N -time-point measurement time series, with $N > 2\max(f_{\text{mod}})/\min(\Delta f_{\text{mod}})$
- 3) Inverse problem: reconstruct time series of N tomographic images
- 4) Post-processing: for every pixel, compute temporal Fourier transform (FT) of the reconstructed $\mu_a(t)$.
- 5) Post-processing: create spatial map of FT amplitude at each f_{mod} .

obtained from the same sets of detector readings but employing different varieties of a reconstruction algorithm. Importantly, in principle the reconstruction methods should produce identical results; there is no self-evident *a priori* reason for choosing to use one rather than the other. However, application of the FESI method indicates that one variety can produce spatially accurate images of perturbations at any location of the modeled medium, and the other can not do so. Finally, it can be tentatively suggested that the computed ISF for either algorithm affords a way of applying a spatial deconvolution correction to a reconstructed image.

2. Results/Conclusions

A regularly-shaped two-dimensional medium was chosen for the initial demonstration of concept. As shown in Figure 3, the phantom is a homogeneous disk of 8 cm diameter, with optical coefficient values of $\mu_a = 0.06 \text{ cm}^{-1}$, $\mu_s' = 10 \text{ cm}^{-1}$. For more convenient solution of the forward and inverse problems, the mathematical boundary of the disk was extended 0.5 cm beyond that of the “physical” medium, as indicated in the Fig. 3; the coefficient values in the extended region are the same as those of the “physical” medium. Sixteen equally spaced, unit-strength, homogeneous point sources were placed in the medium at the indicated positions on the physical boundary.

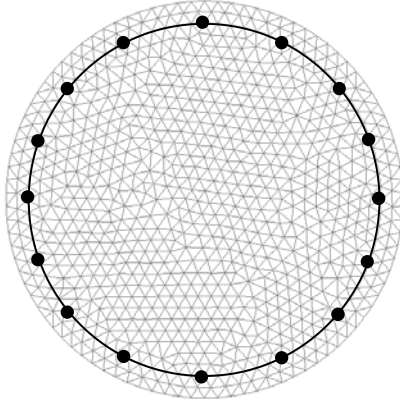


Figure 3: Model medium. μ_a is modulated at a different frequency in each finite element. Black circle indicates “physical” boundary. Black dots indicate source/detector locations.

largest f_m , a time series of ten thousand sets of tomographic detector readings was computed, with $\Delta t = 0.01 \text{ s}$. Image reconstruction was carried out with two algorithms, both based on a singular-value decomposition (SVD) of the image operator matrix. The first algorithm used was the previously described weight-transform SVD (SVDWT) method [8]. The second reconstruction method — SVDWTWRS — combined SVDWT with an additional matrix preconditioning operation, in which each equation was scaled so that all rows of the weight matrix had the same sum.

Two types of analysis were performed on the 1,604 FT amplitude maps produced in step five of the computation (see Fig. 2). First, the global spatial correlation was computed between each amplitude map and the known spatial distribution of the corresponding frequency in the target medium (ideal result: correlation exactly equal to 1.0 at all frequencies). Second, the coordinates of each map’s center-of-mass were computed, from which we easily determined its displacement from the geometric centroid of the finite element whose μ_a was modulated at the corresponding frequency (ideal result: displacement exactly equal to 0.0 at all frequencies). These two quantities are plotted, as a function of f_m (or, equivalently, location in the target medium), for the SVDWT algorithm in Figure 4, and for the SVDWTWRS algorithm in Figure 5. The lighter-colored curve in each panel is derived from the unfiltered FT amplitude spatial distributions. The darker curve is the result obtained when the calculations were repeated after we made the best-possible correction consistent with a particular theoretical model, according to which the amplitude maps derived from the reconstructed images are a simple linear transformation of the true spatial distributions present in the target medium.

Casual inspection of Figs. 4 and 5 reveals that each plotted function exhibits a qualitative change in behavior after the 400th f_m . The change is simply a consequence of the fact that the first 400 finite elements all were located in the zone (see Fig. 3) lying between the physical and extended boundaries, i.e., outside the ring of sources and detectors. Closer inspection of Fig. 4 reveals that both spatial accuracy measures fall particularly far from their ideal values for those finite elements corresponding to roughly the 800th through 1100th f_m . These elements are the ones that lay in the central region of the target medium. That is, the SVDWT algorithm reconstructed images that were strongly distorted spatially, with the absorption coefficient values of the central region significantly displaced toward the surface while those of the more peripheral region were recovered with considerably greater accuracy. In contrast, the spatial correlation and centroid displacement are considerably more spatially uniform for the amplitude maps derived from the images reconstructed by the (preconditioned) SVDWTWRS algorithm. This is a significant

observation, as the two reconstruction variants theoretically should yield the same solution when both operate on a given set of detector data. Finally, it is seen that in each panel of Fig. 4 and Fig. 5, most points on the dark (corrected images) curve lie closer to the ideal value than those on the light (uncorrected images) curve. This suggests the possibility that information in the ISF could be used to perform post-reconstruction enhancement of the images' spatial accuracy.

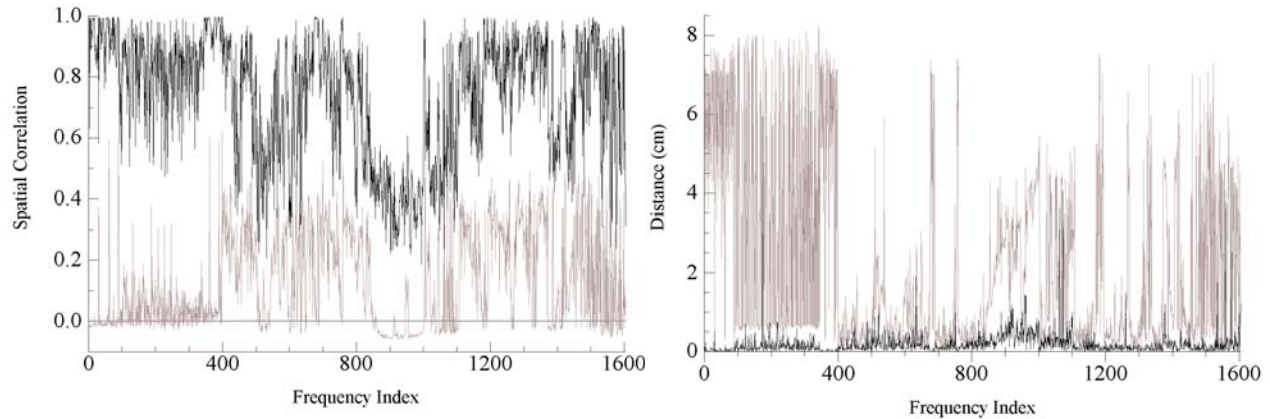


Fig. 4. Global spatial correlation (left) and distance of centroid from the correct location, for all spatial maps of FT amplitude derived from images reconstructed using the SVDWT algorithm.

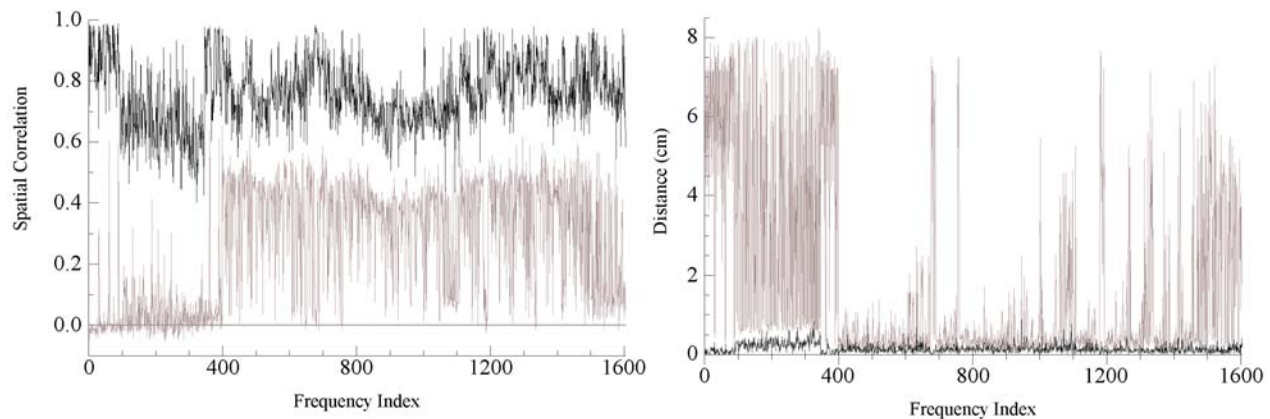


Fig. 5. Global spatial correlation (left) and distance of centroid from the correct location, for all spatial maps of FT amplitude derived from images reconstructed using the SVDWTWRS algorithm.

3. References

- [1] Y. Pei, H. L. Graber, and R. L. Barbour, "Influence of systematic errors in reference states on image quality and on stability of derived information for DC optical imaging," *Appl. Opt.* **40** 5755–5769 (2001).
- [2] Y. Pei, H. L. Graber, and R. L. Barbour, "Normalized-constraint algorithm for minimizing inter-parameter crosstalk in DC optical tomography," *Optics Express* **9**, 97–109 (2001).
- [3] C. H. Schmitz, H. L. Graber, H. Luo, I. Arif, J. Hira, Y. Pei, A. Bluestone, S. Zhong, R. Andronica, I. Soller, N. Ramirez, S.-L. S. Barbour, and R. L. Barbour, "Instrumentation and calibration protocol for imaging dynamic features in dense-scattering media by optical tomography," *Applied Optics* **39**, 6466–6486 (2000).
- [4] C. H. Schmitz, Y. Pei, H. L. Graber, J. M. Lasker, A. H. Hielscher, and R. L. Barbour, "Instrumentation for Real-Time Dynamic Optical Tomography," in *Photon Migration, Optical Coherence Tomography, and Microscopy*, Stefan Andersson-Engels, Michael Kaschke, eds., Proc. SPIE 4431, 282–291 (2001).
- [5] C. H. Schmitz, M. Löcker, J. M. Lasker, A. H. Hielscher, and R. L. Barbour, "Instrumentation for fast functional optical tomography," *Review of Scientific Instruments*, in press (2002).
- [6] H. L. Graber, C. H. Schmitz, Y. Pei, S. Zhong, S.-L. S. Barbour, S. Blattman, T. Panetta, and R. L. Barbour, "Spatio-temporal imaging of vascular reactivity," in *Physiology and Function from Multidimensional Imaging*, A. V. Clough, C.-T. Chen, eds., Proc. SPIE 3978, 32–43 (2000).
- [7] R. L. Barbour, H. L. Graber, Y. Pei, S. Zhong, and C. H. Schmitz, "Optical tomographic imaging of dynamic features of dense-scattering media," *J. Opt. Soc. Am. A* **18**, 3018–3036 (2001).
- [8] E. Y. Lin, Y. Wang, Y. Pei, and R. L. Barbour, "Solution of the Perturbation Equation in Optical Tomography Using Weight Functions as a Transform Basis," in *Advances in Optical Imaging and Photon Migration (OSA Trends in Optics and Photonics, Vol. XXI)*, J. G. Fujimoto, M. S. Patterson, eds., (Optical Society of America, Washington, DC, 1998), pp. 197–202.